INTERNATIONAL JOURNAL FOR NUMERICAL METHODS IN FLUIDS
*Int. J. Numer. Meth. Fluids* 2002; **40**:1471–1484 (DOI: 10.1002/fld.405)

# Putting domain decomposition at the heart of a mesh-based simulation process

Peter Chow*,† and Clifford Addison

*Fujitsu Laboratories of Europe Limited, Hayes Park Central, Hayes End Road, Hayes, Middlesex UB4 8FE, U.K.*

SUMMARY

In computational mechanics analyses such as those in computational fluid dynamics and computational structure mechanics, some 60–90% of total modelling time is taken by specifying and creating the model of the geometry and mesh. The rest of the time is spent in actual analyses and interpreting the results. This is especially true for industries such as aerospace and electronics, where 3D geometrically complex models with multiple physical processes are common. Advances in computational hardware and software have tended to increase the proportion of time spent in model creation, partly because such advances have made it feasible to solve hard and complex geometry problems in a timely fashion. This paper shows one way to exploit the advances in computation to reduce the model creation time and potentially the overall modelling time, namely the use of domain decomposition to define consistent and coherent global models based on existing component geometry and mesh models. In keeping with existing modelling processes the re-engineering cost for the process is minimal. Copyright © 2002 John Wiley & Sons, Ltd.

KEY WORDS: domain decomposition; computational mechanics; mesh-based simulation

## INTRODUCTION

Figure 1 show a mesh-based computational mechanics (CM) and engineering design and optimization process regularly found in the manufacturing industries. Like most manufacturing processes the cost of the change needs to be weighed against the associated benefits. Naturally, only cases where the benefits outweigh the cost of changing will be considered.

In mesh-based simulations the most time consuming part of the whole process—consuming some 60–90% of total modelling time—is the stage for geometry creation and mesh generation (GCMG). This is the case with almost all of the mesh-based simulation software of today. In the computer aided engineering (CAE) space there is much development towards a CAD data exchange standard to enabled direct importing of geometry data created in CAD into the

*Correspondence to: Peter Chow, Fujitsu Laboratories of Europe Ltd, Hayes Park Central, Hayes End Road, Hayes, Middlesex UB4 8FE, U.K.
†E-mail: p.chow@fle.fujitsu.com

*Received 1 November 2001*
*Revised 12 June 2002*

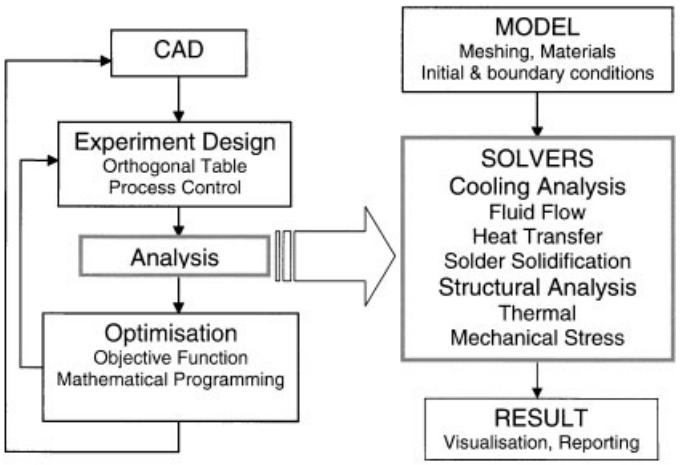


Figure 1. Mesh-based simulation process.

stage of model geometry creation. Together with the development in tools for repairing flawed CAD data (flawed for meshing, not for CAD) for mesh generation, advances in automatic meshing have simplified and speeded up the GCMG stage considerably. Unfortunately, large and complex geometry problems still require a high degree of user intervention and time—thus it remains the most time intensive stage in the whole process. The problem is often made more acute by the physics involved that require a particular degree of mesh density and alignments, and geometric features of contrasting scales. The advances in computational hardware and software technologies have in part kept the GCMG percentage ratio high by aggressively driving the analysis time down.

The concept of our novel approach, which we refer to as component meshing and gluing (CMG), is to create and solve individual parts (sub-models) that make up the model. The solution is arrived at by the exchange of boundary conditions between the parts. The parts (components) are created and meshed individually in the same way as existing models, for example doors, wheels, etc. for automobile parts. Domain decomposition is the 'glue' that ties it all together at the solver stage. Figure 2 shows the modifications necessary to convert an existing mesh-based simulation process to the CMG concept. The new elements are: (1) finding the interface region between two parts and generating a surface mesh for the interface with prescribed points at the model creation stage. The methods for doing these tasks are commonly found in solid modelling and mesh generation technologies and (2) incorporating the interface regions and conditions into the existing solution procedure as boundary conditions at the solver stage—this is addressed in this paper.

With the entire model composed from 'decoupled' meshed parts, the compute time at the solver stage will be longer than a coupled model; the solver is similar to that of Block solvers strategy [1–6]. How much longer will depend on the numerical technology employed under the umbrella of the domain decomposition methods. Therefore, if the decoupled mesh solver procedure is not too expensive then for certain types of applications where sub-models and even whole models can be reused, the CMG concept could be of value. The thinking behind the CMG concept is that the GCMG stage could be turned into a 'pick-and-drop' procedure,

 

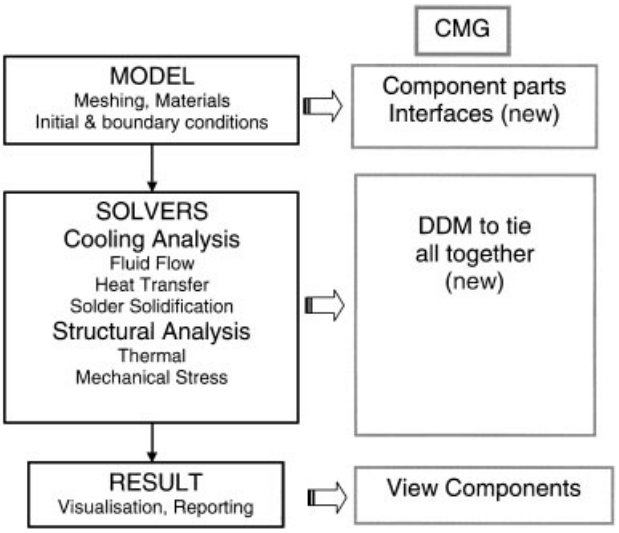


Figure 2. Modified mesh-based simulation process.

picking from a database of meshed parts and dropping the parts into the 'virtual worktop' to form the model with part connectivity information for the solver stage. With this approach, it is possible that model creation would be a fraction of the time it takes to do now and it could offset the extra compute time in the decoupled mesh solver to yield a shorter overall modelling time. This is the main question we try to address in our study—will total modelling time be shortened or not?

## INTERFACE QUANTITIES AND PARTIAL DIFFERENTIAL EQUATION SOLVED

The domain decomposition methods (DDM) are divided into two main classes, overlapping and non-overlapping of the boundary regions. In the overlapping case the domains overlap with each other, while the non-overlapping domains share an interface. With CMG, the non-overlapping class of methods is used. For more information on DDM and its applications the readers are directed to the DDM series in sciences and engineering [7, 8].

In the present study the discretization used is the unstructured cell-centred finite volume method (FVM) with polyhedral control volumes [9–12]. Due to the FVM's conservation properties, the interface regions by venture need to be conserved also. The introduction of an interface surface mesh provides the means and flexibility to achieve this property, and maintain the relationship between elements of the neighbouring domains. Therefore, for each element on the interface surface there is a one-to-one association between neighbour domain elements with the quantities at the interface. The interface condition here is that both the unknown conserved variable ($U$) and its gradient ($\nabla U$) are continuous. The subscripts L and R are the left and right neighbour domain, respectively,

$$U_{\mathrm{L}} = U_{\mathrm{R}} : \nabla U_{\mathrm{L}} = \nabla U_{\mathrm{R}} \tag{1}$$

 

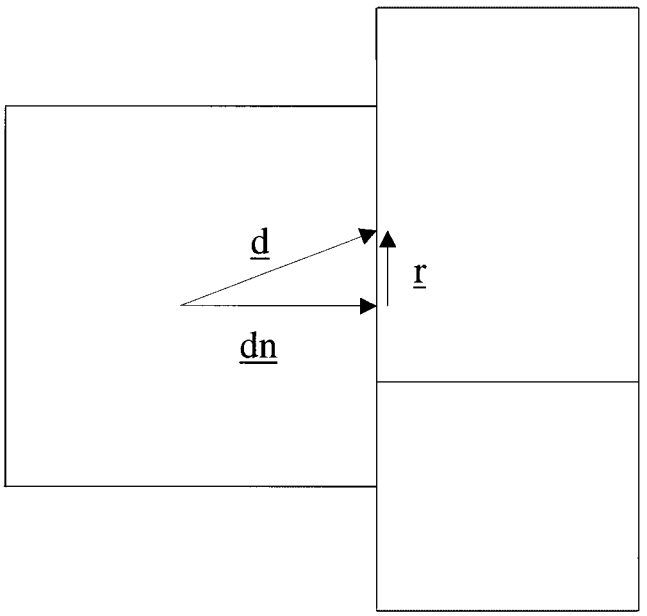


Figure 3. Vector association to element at interface.

The interface quantities (denoted by the subscript I) $U_I$ and $\nabla U_I$ are calculated from the following equations, with $\Delta N$ the normal distance to the interface

$$U_I = \frac{\Delta N_R}{\Delta N_L + \Delta N_R}(U_L^* - U_R^*) + U_R^* \tag{2}$$

$$\nabla U_I = \frac{U_R^* - U_L^*}{\Delta N_L + \Delta N_R} \tag{3}$$

The unknowns with superscript * are derived from Equation (4), adjusting for non-ortho gonality. In the orthogonal case the vector ($\underline{r}$) is zero. Figure 3 shows the vector association of an element to the interface. The vector ($\underline{d}$) is between edge mid-point to element cell-centre and vector ($\underline{dn}$) is the normal vector between element cell-centre and the boundary edge

$$U_L^* = U_L + \{(\text{grad}\, U)\cdot\underline{r}\}_L \tag{4}$$

$$\underline{r} = \underline{d} - \underline{dn} \tag{5}$$

The PDE we are solving in this study is the thermal energy equation, conduction only, in temperature ($T$) form and in two dimensions. The variables in Equation (6) are density ($\rho$), specific heat ($c$), thermal conductivity ($k$), time ($t$) and the source term ($S$)

$$\rho_c \frac{\partial T}{\partial t} = \nabla \cdot (k \nabla T) + S(T) \tag{6}$$

 

The non-linearity is introduced in the form of a material phase-change in the source term. For solidification using the enthalpy source-based method this is given by Equation (7) with latent heat ($L$) and liquid fraction ($f$).

$$S(T) = \rho L \frac{\partial f(T)}{\partial t} \tag{7}$$

The algorithm for solving these kinds of problems is discussed in papers by Chow and Cross [13] and Voller and Swaminathan [14] and will not be detailed here. For boundaries that coincide with the domain interface a blending of the Dirichlet and Neumann boundary conditions is applied, see Equation (8), with $\beta$ being the blending factor between 0 and 1. A blending value of 0.5 has been found to be stable and has a good rate of convergence for the experimental cases conducted. The normal Neumann boundary condition would have been the simplest way to preserve flux quantities across the interface and between the domains. Unfortunately, this could lead to a situation where the system of equations has multiple solutions; the blending of Dirichlet and Neumann is a way to overcome this problem and assure conservation when convergence is achieved. Equation (9) gives the thermal conductivity at the interface using geometric averaging; alternatively harmonic averaging can be used in the composite material case.

$$\frac{\partial T}{\partial n} = \beta \frac{T_{\mathrm{I}} - T_{\mathrm{R}}^*}{\nabla N_{\mathrm{R}}} + (1-\beta)\nabla T_{\mathrm{I}} \tag{8}$$

$$k_{\mathrm{I}} = \frac{\Delta N_{\mathrm{R}}}{\Delta N_{\mathrm{L}} + \Delta N_{\mathrm{R}}} (k(T_{\mathrm{L}}^*) - k(T_{\mathrm{R}}^*)) + k(T_{\mathrm{R}}^*) \tag{9}$$

In the calculation of element gradients in each domain, the mid-point edge value is needed for each edge. When the boundary edge coincides with the interface, the mid-point edge value ($T_{\mathrm{E}}$) is calculated using Equation (10), with $S$ the surface area. In the matching grid case the edge $T_{\mathrm{E}}$ has the interface value $T_{\mathrm{I}}$. For boundary edges that partially coincide with the interface, weighted average is used to provide the mid-point edge value

$$T_{\mathrm{E}} = \frac{\sum_{f=1}^{n} (T_{\mathrm{I}} S_{\mathrm{I}})_f}{S_{\mathrm{E}}} \tag{10}$$

When compared with the latest developments in DDM [7, 8] this is not the most effective way to obtain fast convergence but the priority in this paper is conserving quantities across the interface. Enhancements to the approach are underway and are still in keeping with preserving conservation of quantities.

The solution procedure for CMG is as follow:

1. calculate interface quantities such as fluxes from initial conditions;
2. solve each domain independently with latest interface quantities;
3. evaluate interface quantities for each interface surface;
4. repeat from (2) if not converged on all interfaces and domains.

This is similar to a Block solver procedure [1–6], where each block's computation is commonly performed separately and the solution in one block provides the boundary conditions to the adjoining blocks.

 

When the model consists of a single domain (part) then stages 1 and 3 are redundant, thereby reverting back to the conventional solution procedure. In the numerical experiments conducted in the next section, the single coupled mesh cases were performed in this way and refer to it as CMG-coupled (for multiple domains it is CMG-DDM). From the procedure both the domain and interface elements can be computed in parallel within each stage without data conflicts. This implies the solutions by parallel and scalar computations are identical on homogeneous systems; no investigation has yet been done on the parallel aspects of the procedure in the present study.

## NUMERICAL EXPERIMENTS

The physical model example taken for the experiment has the characteristics commonly found in electronic packaging applications—chips, solder bumps, boards. The basic components—chips, solder bumps, pads and boards—are of simple geometry, individually. It is when these components are used in combination that the geometry model becomes intricate and complex. The solder bumps bonding the chip to the board are main areas of interest, especially in manufacturing and in the operational life of the electronic component.

Three numerical experiments were conducted using the same geometry model, see Figure 4. The experiments are: (A) a linear steady state problem, (B) a non-linear problem with phase-change occurring inside the domain, and (C) a non-linear problem with a moving front travelling across the domains. Figure 5 show the three mesh configurations used: (1) matching grid at interface, and non-matching at interface for (2) and (3) with different degrees of coarseness and element aspect ratios. The meshes may be coarse but they are in common with the application. Engineers in most instances want the coarsest mesh they can use without significant lost of accuracy, especially in chip and board regions, for fast analysis and modelling to meet the short time-to-market window. In cases (2) and (3) polyhedral or arbitrary control volume [10, 11] is used for the single coupled mesh situation. The decoupled model consists of four domains, chip, board and two connectors. There are a total of four interface regions.

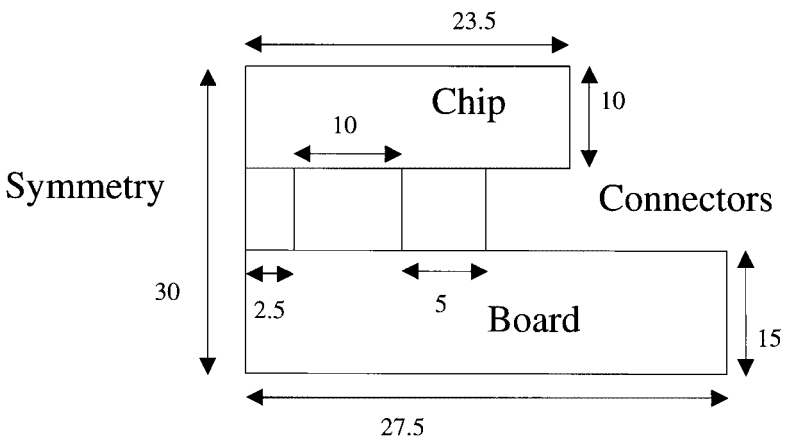


Figure 4. Model problem.

 

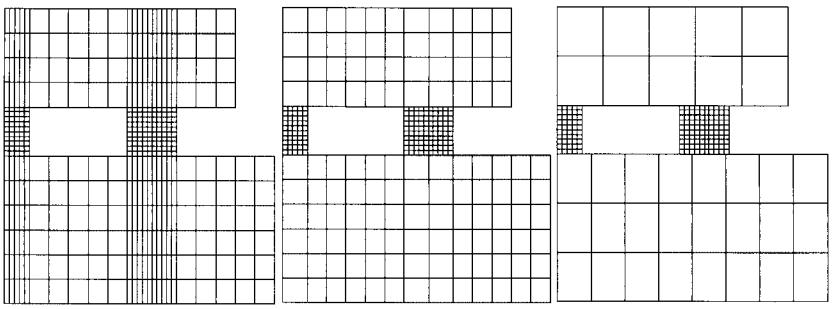


Figure 5. Mesh configurations.

For each connector there is an interface for connector-and-chip and connector-and-board. The last numerical experiment is not a physical process in electronic packaging but an arbitrary academic model to provide a better insight of any ill interface effects by modelling a moving front across the boundary interfaces.

It is not possible to give an accurate measure of the total modelling time at this point. No pick-and-drop environment is in place for creating the models. The separated mesh models have all been created with some manual intervention, notably the interface connectivity. There are precise timings for the analysis. By treating the CMG-coupled timing as the time required for the analysis, then a total modelling time can obtained by assuming analysis time is a certain proportion of total modelling time. By comparing this proportion to the ratio of the CMG-coupled analysis time to the CMG-DDM analysis time, it is possible to draw some conclusions on the competitive nature of the CMG-DDM approach and how aggressive the pick-and-drop timing needs to be. In the numerical experiments below, 10% is taken as the proportion for the CMG-coupled analysis time—10:90 (analysis to model creation) ratio. If the ratio of CMG-DDM time to CMG-coupled time is more than a factor of 10, then the CMG-DDM approach is not competitive because the total modelling time for CMG-DDM will be larger than that for CMG-coupled even with zero time spent in the pick-and-drop phase. In all of the following experiments, the results obtained for the CMG-coupled approach with mesh Case 1 provide the reference values against which the other cases are compared.

All the contour plots below are plotted using cell-centred (element) values for a precise comparison of solutions. A duel-mesh was created for each of the mesh models, see Figure 6, for the contour plotting.

### *Experiment A: linear steady state*

Figure 7 shows the results of both the coupled (CMG-coupled) and decoupled (CMG-DDM) cases. The boundary conditions for this are: chip top is a Dirichlet boundary, cold at $T = 10$ (Celsius), board bottom is a Dirichlet boundary, hot at $T = 100$, with a convective boundary for the rest ($T$-ambient=25 with a heat transfer coefficient of $H = 1$). The material properties used are density ($\rho = 100$), thermal conductivity ($k = 1$), and specific heat ($c = 1$). From the plots, the coupled and decoupled results are virtually indistinguishable. For mesh Case 1 the results are identical up to seven decimal places. Table I gives the total energy in the

 

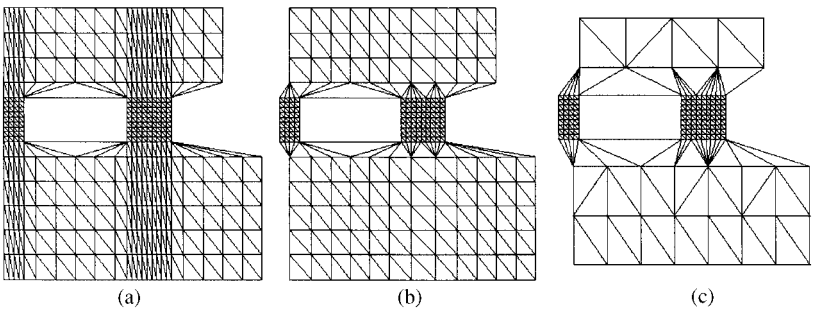


Figure 6. Three duel-mesh cases.

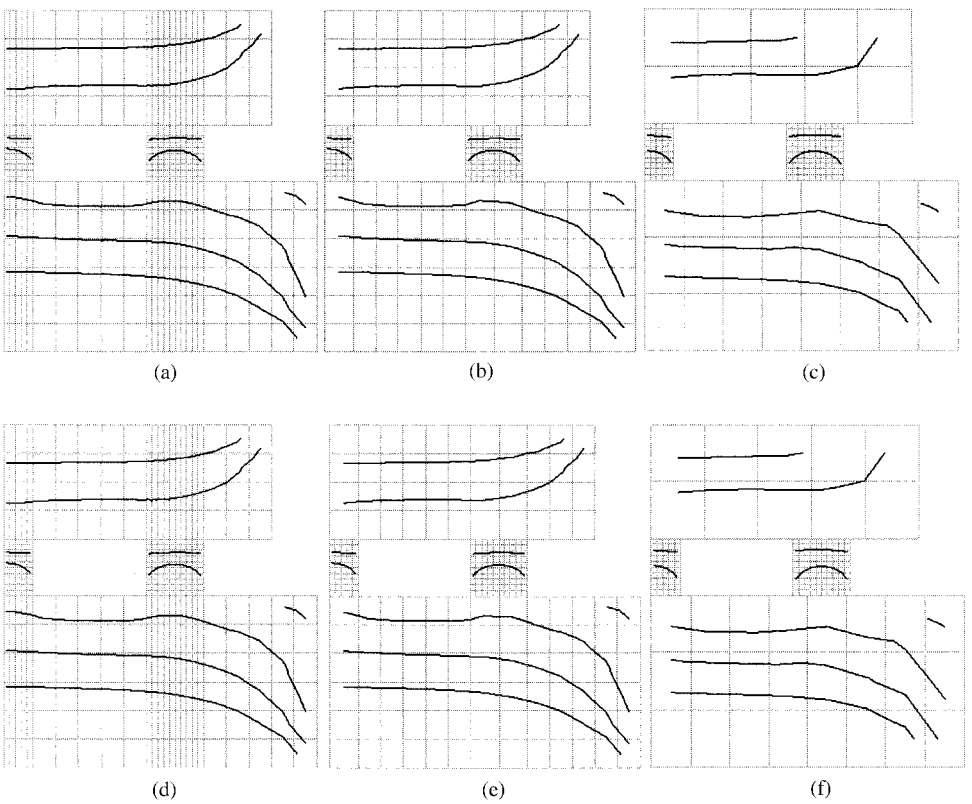


Figure 7. Result of Experiment A. Contour plotted at level 15, 20, 25, 26, 35, 50 and 65. Plots a, b and c are computed by CMG-coupled and d, e and f are computed by CMG-DDM.

system for all the cases. Case 1, CMG-coupled, is the reference case for solution accuracy and computing costs. The data indicates that the biggest solution deviation from reference case is less than 5 per cent in the coarsest mesh case. As expected, the time for CMG-DDM is much slower, about 15, 11.7 and 9.8 times more costly for the respective mesh cases. This means

 

Table I. Total energy and timings of Experiment A.

| Mesh model case | Total energy | Relative error | CPU time | Time factor |
|---|---|---|---|---|
| Case 1 | 2.886712251E+06 | | 0.20 | |
| CMG-DDM | 2.886712247E+06 | 1.386E−09 | 3.00 | 15.00 |
| Case 2 | 2.888806114E+06 | 7.253E−04 | 0.36 | 1.80 |
| CMG-DDM | 2.887191289E+06 | 1.659E−04 | 2.34 | 11.70 |
| Case 3 | 2.767585689E+06 | 4.127E−02 | 0.23 | 1.15 |
| CMG-DDM | 2.837320587E+06 | 1.711E−02 | 1.96 | 9.80 |

the values have breached or nearly breached the yardstick guide and indicate the CMG-DDM is totally uncompetitive. Although the last value is below the factor of 10 yardstick-mark, it is too close and the pick-and-drop phase is unlikely to meet such an extreme time constraint.

*Experiment B: non-linear transient—phase-change occurring inside domain*

This is a cooling problem in which the solder bump material undergoes a phase-change, in this instance the eutectic temperature is set at $T = 80$ for solidification from liquid to solid with both the board and chip remaining solid throughout. A Dirichlet boundary condition, $T = 25$, is applied to all external boundaries with the board bottom having a Dirichlet value of $T = 100$. The initial temperature for the entire model is set at $T = 100$. The initial temperature is set above the eutectic value and as the problem cools, the solder material solidifies and a moving liquid–solid front occurs inside the domain of the solder bumps. The material properties used are density ($\rho = 1000$), thermal conductivity ($k = 50$), and specific heat ($c = 100$) for all components with latent heat ($L = 10\,000$) for the solder.

Figures 8 and 9 show the results of the temperature and liquid-fraction, respectively, for the CMG-coupled and CMG-DDM cases. Due to the phase-change, latent heat energy is released and with both chip and board being cooler, heat transfer from solder bumps to both chip and board occurs. The temperature plots are indistinguishable between the CMG-coupled and CMG-DDM for the matching grid, a notable difference for non-matching grid cases in elements near the interfaces. The liquid-fraction plots show a slight difference, about a cell width in the solder, between the three cases and virtually the same between the CMG-coupled and CMG-DDM for all cases. Table II has the total energy in the system for all the cases, with mesh model Case 1 the reference case for accuracy and computing costs. The biggest solution deviation from the reference case is under 5 per cent in the coarsest case. The time for CMG-DDM is 4.7, 4.8 and 3.3 times more costly for the respective mesh cases. It is not clear why the second timing is slightly higher than the first as it was expected to be lower, investigation is ongoing to comprehend this. All the values are still well below the yardstick guide and indicate the CMG-DDM has some possibility to be competitive. The first two values indicate they could be competitive even at the 20:80 ratio level and the last value could be competitive at the 30:70 ratio level.

*Experiment C: non-linear transient—moving front travelling across domains*

In the final experiment a liquid–solid moving front is initiated at the top of the chip and made to travel across the solder bumps and through into the board. The initial condition is that all

 

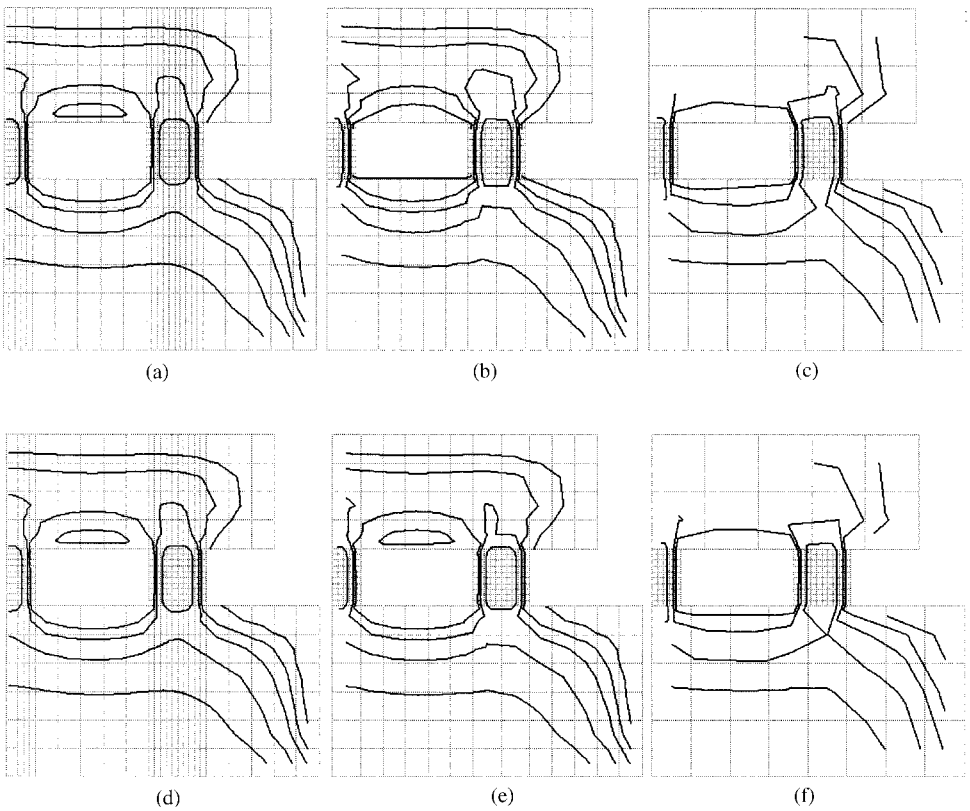


Figure 8. Temperature plots of Experiment B. Contour plotted at level 40, 50, 60, 75 and 90. Plots a, b and c are computed by CMG-coupled and d, e and f are computed by CMG-DDM.

the domains are solids with an initial temperature value $T = 75$ below that of the eutectic melt temperature $T = 80$. A high-energy source is applied on the top surface of the chip in the form of a hot Dirichlet boundary condition $T = 500$. The board bottom is kept cool with a Dirichlet value $T = 0$ and the rest of the external boundary has an adiabatic condition. The material properties used are density ($\rho = 1000$), thermal conductivity ($k = 50$), specific heat ($c = 100$), and latent heat ($L = 100$).

Figure 10 shows the liquid-fraction results of mesh Case 1 for both CMG-coupled and CMG-DDM. The time sequence, $T1$, $T2$ and $T3$, show the positions of the front, before moving into connectors, inside connectors and through into the board, respectively. Likewise, Figure 11 shows the results of mesh Case 2. In mesh Case 1 the solution is indistinguishable between CMG-coupled and CMG-DDM plots. For mesh Case 2, there is a notable difference in the end plot of the liquid-fraction. As with Experiment B, it is about a cell width difference. Table III has the total energy in the system for all the cases, with Case 1 the reference case for accuracy and computing costs. The biggest deviation from the reference case is under 0.25 of a per cent and the time for CMG-DDM is 7.1 and 5.8 times more costly for the respective mesh cases. Both these values are well within the yardstick guide and indicate the CMG-DDM has some potential, but not at the level observed in Experiment B.

 

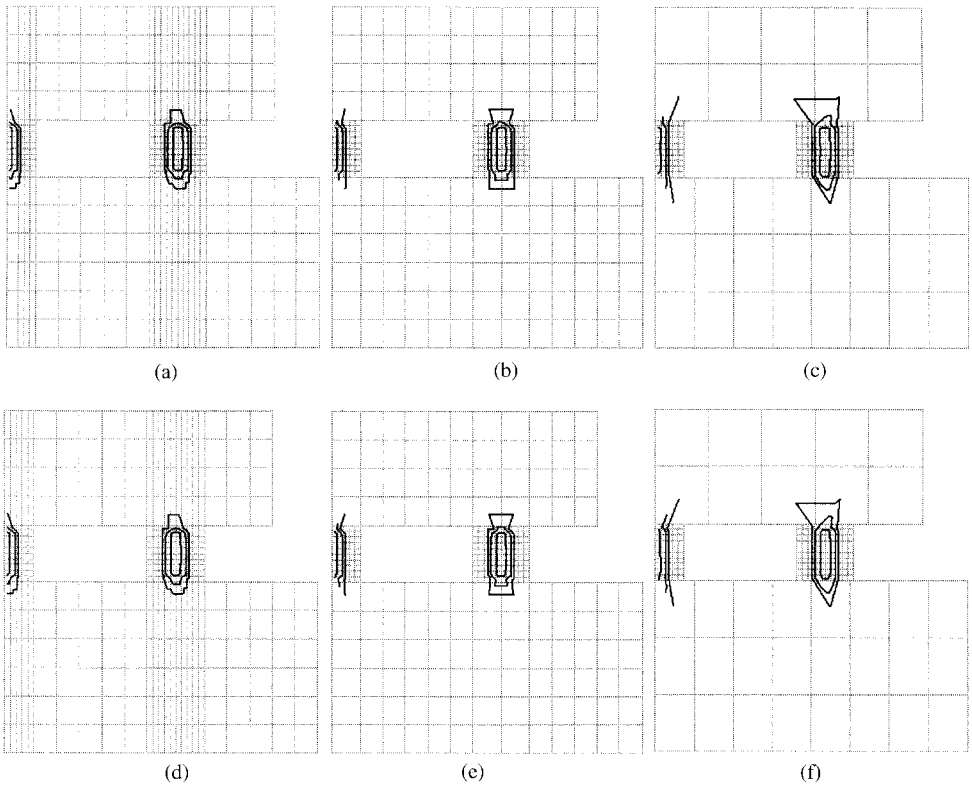


Figure 9. Liquid-fraction plots of Experiment B. Contour plotted at level 0.1, 0.5 and 0.9. Plots a, b and c are computed by CMG-coupled and d, e and f are computed by CMG-DDM.

Table II. Total energy and timings of Experiment B.

| Mesh model case | Total energy | Relative error | CPU time | Time factor |
|---|---|---|---|---|
| Case 1 | 4.582046446E+09 | | 1.65 | |
| CMG-DDM | 4.582047328E+09 | 1.925E−07 | 7.77 | 4.71 |
| Case 2 | 4.639836819E+09 | 1.261E−02 | 5.57 | 3.38 |
| CMG-DDM | 4.585301262E+09 | 7.103E−04 | 7.90 | 4.79 |
| Case 3 | 4.789205851E+09 | 4.521E−02 | 4.19 | 2.54 |
| CMG-DDM | 4.798140580E+09 | 4.716E−02 | 5.39 | 3.27 |

The values indicate they could be competitive even at the 14:86 and 17:83 ratio level, respectively.

## SUMMARY

From the results obtained, putting domain decomposition at the heart of a mesh-based simulation process, like the CMG concept, is not competitive for steady state linear problems.

 

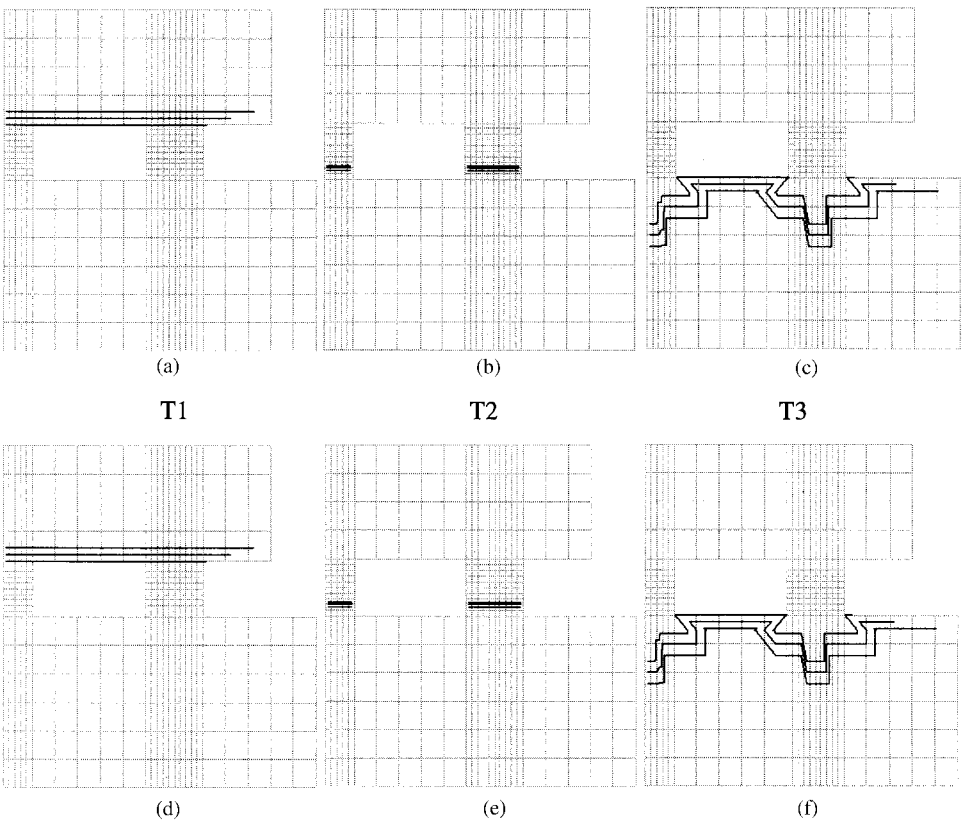


Figure 10. Result of Experiment C—Case 1. Contour plotted at level 0.1, 0.5 and 0.9. Plots a, b and c are computed by CMG-coupled and d, e and f are computed by CMG-DDM.

Table III. Total energy and timings of Experiment C.

| Mesh model case | Total energy | Relative error | CPU time | Time factor |
|---|---|---|---|---|
| Case 1 | 1.941690115E+10 | | 7.85 | |
| CMG-DDM | 1.941690128E+10 | 6.695E−09 | 55.36 | 7.05 |
| Case 2 | 1.941710882E+10 | 1.070E−05 | 17.88 | 2.28 |
| CMG-DDM | 1.936855500E+10 | 2.490E−03 | 45.62 | 5.81 |

On non-linear transient problems, the results suggest some possible potentials for shortening the total modelling time with the CMG concept and merit further investigations. If more advanced DDM technology can achieve more aggressive timings and the 'pick-and-drop' model creation can be realized then the CMG concept could be of important value to the mesh-based simulation process. It is clear also that the CMG-coupled approach can also benefit from the pick-and-drop model by either bonding the separated mesh components together into a single mesh (requiring a mesh bonding technology) or an implicit block solver strategy, with the

 

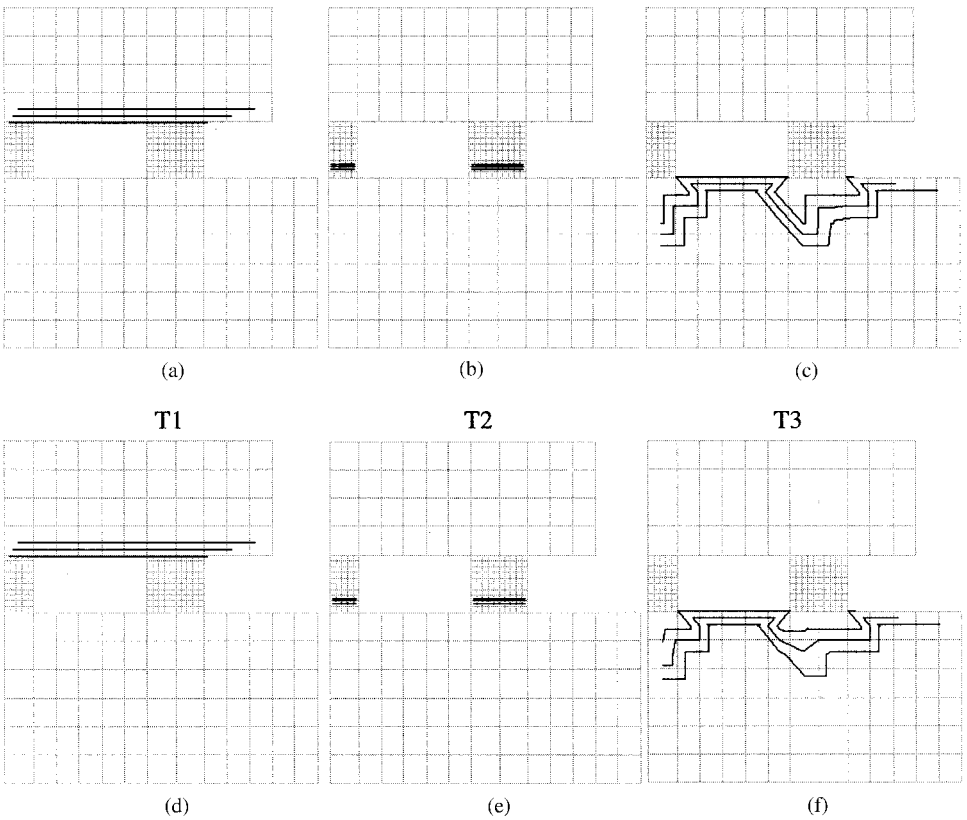


Figure 11. Result of Experiment C—Case 2. Contour plotted at level 0.1, 0.5 and 0.9. Plots a, b and c are computed by CMG-coupled and d, e and f are computed by CMG-DDM.

unstructured finite volume approach. The downside to this is it may not be flexible enough for other methods or solution strategies.

## REFERENCES

1. Pang CY, Street RL. A coupled multigrid-domain-splitting technique for simulating incompressible flow in geometrically complex domains. *International Journal for Numerical Methods in Fluids* 1991; **13**:269–286.
2. Zang Y, Street RL. A composite multigrid method for calculating unsteady incompressible flows in geometrically complex domains. *International Journal for Numerical Methods in Fluids* 1995; **20**:341–361.
3. Hubbard BJ, Chan HC. A Chimera scheme for incompressible viscous flows with applications to submarine hydrodynamics. AIAA paper 94-2210, 1994.
4. Coelho P, Pereira JCF, Carvalho MG. Calculation of laminar recirculating flow using a local non-staggered gird refinement system. *International Journal for Numerical Methods in Fluids* 1991; **12**:535–557.
5. Lilek Z, Muzaferija S, Peric M, Seidl V. An implicit finite-volume method using non-matching blocks of structured grid. *Numerical Heat Transfer*, *Part B* 1997; **32**:385–401.
6. Lilek Z, Muzaferija S, Peric M, Seidl V. Computation of unsteady flows using non-matching blocks of structured grid. *Numerical Heat Transfer*, *Part B* 1997; **32**:403–418.
7. Lai C-H, Bjorstad PE, Cross M, Widlund (eds). *Domain Decomposition Methods in Sciences and Engineering*. DDM.org, Greenwich, UK, 1999.
8. Chan T, Kako T, Kawarada H, Pironneau O (eds). *Domain Decomposition Methods in Sciences and Engineering*. DDM.org, Chiba, Japan, 2001.

 

9. Hirsch C. *Numerical Computation of Internal and External Flows*, vol. 1. Wiley: New York, 1989.
10. Demirdzic I, Lilek Z, Peric M. A colocated finite volume method for predicting flows at all speeds. *International Journal for Numerical Methods in Fluids* 1993; **16**:1029–1050.
11. Chow P, Cross M, Pericleous K. A natural extension of the conventional finite volume method into polygonal unstructured meshes for CFD application. *Applied Mathematical Modelling* 1996; **20**:170–183.
12. Ferziger JH, Peric M. *Computational Methods for Fluid Dynamics*. Springer: Berlin, 1997.
13. Chow P, Cross M. An enthalpy control volume-unstructured mesh (cv-um) algorithm for solidification by conduction only. *International Journal for Numerical Methods in Engineering* 1992; **35**:1849–1870.
14. Voller V, Swaminathan C. General source-based methods for solidification phase change. *Numerical Heat Transfer*, *Part B* 1991; **19**:175–190.

 